PROCEEDINGS OF SPIE

SPIEDigitalLibrary.org/conference-proceedings-of-spie

Ion emission from plasmas produced by femtosecond pulses of short-wavelength free-electron laser radiation focused on massive targets: an overview and comparison with long-wavelength laser ablation

Josef Krása, Vincenzo Nassisi, Tomáš Burian, Věra Hájková, Jaromír Chalupský, et al.

Josef Krása, Vincenzo Nassisi, Tomáš Burian, Věra Hájková, Jaromír Chalupský, Šimon Jelínek, Kateřina Frantálová, Michal Krupka, Zuzana Kuglerová, Sushil Kumar Singh, Vojtěch Vozda, Luděk Vyšín, Jan Wild, Michal Šmíd, Pablo Perez-Martin, Xiayun Pan, Marion Kühlman, Juan Pintor, Jakub Cikhardt, Matthias Dreimann, Dennis Eckermann, Felix Rosenthal, Sam M. Vinko, Alessandro Forte, Thomas Gawne, Thomas Campbell, Shenyuan Ren, YuanFeng Shi, Trevor Hutchinson, Oliver Humphries, Thomas Preston, Mikako Makita, Motoaki Nakatsutsumi, Alexander Köhler, Marion Harmand, Sven Toleikis, Kateřina Falk, Libor Juha, "Ion emission from plasmas produced by femtosecond pulses of short-wavelength free-electron laser radiation focused on massive targets: an overview and comparison with long-wavelength laser ablation," Proc. SPIE 12578, Optics Damage and Materials Processing by EUV/X-ray Radiation (XDam8), 125780J (6 June 2023); doi: 10.1117/12.2670113

SPIE.

Event: SPIE Optics + Optoelectronics, 2023, Prague, Czech Republic

Ion emission from plasmas produced by femtosecond pulses of short-wavelength free-electron laser radiation focused on massive targets: an overview and comparison with long-wavelength laser ablation

Josef Krása*[a], Vincenzo Nassisi[b,c], Tomáš Burian[a,d], Věra Hájková[a], Jaromír Chalupský[a], Šimon Jelínek[a,d,e], Kateřina Frantálová[a], Michal Krupka[a,d,f], Zuzana Kuglerová[a,e], Sushil Kumar Singh[a,d], Vojtěch Vozda[a], Luděk Vyšín[a], Jan Wild[e], Michal Šmíd[g], Pablo Perez-Martin[g], Xiayun Pan[g,h], Marion Kühlman[i], Juan Pintor[j], Jakub Cikhardt[k], Matthias Dreimann[l], Dennis Eckermann[l], Felix Rosenthal[l], Sam M. Vinko[m,n], Alessandro Forte[m], Thomas Gawne[m], Thomas Campbell[m], Shenyuan Ren[m], YuanFeng Shi[m], Trevor Hutchinson[o], Oliver Humphries[p], Thomas Preston[p], Mikako Makita[p], Motoaki Nakatsutsumi[p], Alexander Köhler[g], Marion Harmand[j], Sven Toleikis[i], Kateřina Falk[a,g,h], Libor Juha[a]

[a] Department of Radiation and Chemical Physics, Institute of Physics, Czech Academy of Sciences, Na Slovance 2, 182 21 Prague 8, Czech Republic
[b] Dipartimento di Matematica e Fisica "E. De Giorgi", Universitá del Salento, Lecce, Italy;
[c]Istituto Nazionale di Fisica Nucleare, Sezione di Lecce, Via per Arnesano, s.n., Lecce, Italy
[d]Laser Plasma Department, Institute of Plasma Physics, Czech Academy of Sciences, Za Slovankou 3, 182 00 Prague 8, Czech Republic
[e]Department of Surface and Plasma Science, Faculty of Mathematics and Physics, Charles University, V Holešovičkách 2, 180 00 Prague 8, Czech Republic
[f]Department of Physical Electronics, Faculty of Nuclear Science and Engineering Physics, Czech Technical University in Prague, V Holešovičkách 2, 180 00 Prague 8, Czech Republic
[g] Helmholtz-Zentrum Dresden-Rossendorf, Bautzner Landstraße 400, Dresden, Germany
[h]Technische Universität Dresden, 01062 Dresden, Germany
[i]DESY Photon Science, Notkestraße 85, D-22607 Hamburg, Germany
[j]Institut de minéralogie, de physique des matériaux et de cosmochimie, UMR 7590 - UPMC/CNRS/IRD/MNHN, Sorbonne Université, 4 place Jussieu, 75005 Paris, France
[k]Department of Physics, Faculty of electrical Engineering, Czech Technical University in Prague, Technická 2, 166 27 Prague 6, Czech Republic
[l]Center for Soft Nanoscience, University of Münster, Busso-Peus-Straße 10, D-48149 Münster, Germany
[m]Department of Physics, Clarendon Laboratory, University of Oxford, Parks Road, Oxford OX1 3PU, UK
[n]Central Laser Facility, STFC Rutherford Appleton Laboratory, Didcot OX11 0QX, UK
[o]Lawrence Livermore National Laboratory, 7000 East Avenue, Livermore, CA 94550, USA
[p]European XFEL GmbH, Holzkoppel 4, D-22869 Schenefeld, Germany

*krasa@fzu.cz; phone +420 266 05 2619; https://www.fzu.cz/en/home

Optics Damage and Materials Processing by EUV/X-ray Radiation (XDam8), edited by Libor Juha, Saša Bajt, Stéphane Guizard, Proc. of SPIE Vol. 12578, 125780J · © 2023 SPIE
0277-786X · doi: 10.1117/12.2670113

ABSTRACT

We report on ion emission from plasma produced on thick targets irradiated with nanosecond and femtosecond pulses delivered by mid-ultraviolet and soft x-ray lasers, respectively. To distinguish between different ion acceleration mechanisms, the maximum kinetic energy of ions produced under different interaction conditions is plotted versus laser fluence. The transformation of the time-of-flight detector signal into ion charge density distance-of-flight spectra makes it possible to determine the mean kinetic energy of the fastest ion groups based on the influence of the acoustic velocity of ion expansion. This allows obtaining additional characteristics of the ion production. The final energy of the group of fast ions determined using the ion sound velocity model is an order of magnitude larger in the fs-XFEL interaction than in the ns-UV one. On the contrary, the ablation yield of ions in our experiment is seven orders of magnitude greater when applying ns-UV laser pulses, not only due to higher energies of UV laser pulses, but also due to a significant difference in interaction and ion formation mechanisms.

Keywords: Ablation, nanosecond pulses, femtosecond pulses, UV excimer laser, soft-x-ray laser, free-electron laser, ion diagnostics, ion detector function, ion rarefaction, ion acoustic velocity, ion scaling

1. INTRODUCTION

Laser ablation and ionization studies introduced shortly after the development of the first powerful nanosecond lasers opened new fields of applied research such as laser ion sources (LIS) and laser ablation mass spectrometry (LA-MS). The focused laser beam allows the surface of bulk solid samples to be ablated with typical micrometre resolution in terms of lateral and depth dimensions. The laser-matter interaction then leads to atomization, excitation, and ionization of any sample. A portion of this material is transformed into a transient plume of high-temperature vapor and plasma [1,2]. When using ultrashort lasers, the interaction changes. Fundamental differences between the ablation process of short (>1 ps) and ultrashort (<1 ps) pulses affect the properties of LIS and LA-MS [3-5]. Based on the timescales and energy balance of the process underlying the ablation event, ultrashort pulses have been shown to be less thermal and cause less collateral damage to the target surface than longer pulses. The possibility of using ultrashort pulses (<200 fs) delivered by tuneable x-ray free-electron lasers (XFEL) has become another watershed for plasma and hot dense matter research [6]

Laser ablation has been studied under different experimental conditions, where the mechanisms creating the energy distribution of the produced ions were not identical, as reported by many of related studies. However, this complicates the understanding of laser ablation. Gaining new knowledge on ionization efficiency can be based on the compilation of experimental data showing the dependence of e.g., velocity, energy, total charge, and current density of ions on fluence or laser intensity. In this communication we want to report on the observation of the characteristics of ions produced by UV (λ=248 nm, τ =23 ns) and soft x-ray (λ=13.5 nm, τ =100 fs) lasers irradiating bulk solid targets and their comparison with data from other works realized using VIS-NIR, ns-fs lasers.

2. TIME-OF-FLIGHT METHODOLOGY

Summarizing and scaling of experimental results obtained under different experimental conditions is a necessary process for understanding the studied physical processes. In the case of surface ablation by the interaction of laser pulses with the solid target, in addition to scanning the damaged surface, various diagnostics are used to measure radiation emission, ranging from IR radiation to x-rays, as well as the characteristics of emitted electrons, ions and neutral clusters, molecules and atoms. Therefore, experimental data processing methods are necessary for the characterization of experimental results.

Ion analysis is based on the principle of operation of the used detectors. In experiments, ion detectors are generally placed far from the irradiated target. At these distances, the recombination of ions is negligible, the charges are non-interacting, and the ion charges are "frozen". Due to the conservation of the total charge, Q, of the ions emitted into the solid angle $d\Omega$, the charge, dQ, captured by the detector surface, dS, decreases with increasing distance, L, from the target:

$$dQ = Qd\Omega = \frac{Q}{L^2} dS. \quad (1)$$

Since the electric current can be represented as the rate at which charge flows through a given surface localized at L, then the current detected by the ion detector decreases with increasing distance as:

$$\frac{dQ}{dt} \propto \frac{J}{L^3} dS\,. \tag{2}$$

As a result, the signal of a detector with active area S decreases with distance as L^{-3}. This equation is the basic relationship that allows comparing the ion current densities, j_1 and j_2, detected by detectors that are placed in the same direction but at different distances from the target L_1 and L_2, respectively:

$$j_1(L_1, t_1)L_1^3 = j_2(L_2, t_2)L_2^3, \tag{3}$$

where the time scale t_1 is related to t_2 through velocity as $L_1/t_1 = L_2/t_2$. These relations have a practical consequence for the determination of the critical distance L_{cr}. The total charge Q_i carried by ions decreases due to the three-body recombination up to L_{cr}, but passing this critical distance, the "freezing" of ion states occurs and the charge of ions obey the power law (1) for the three-dimensional dilution of the plasma far from the target, as it was experimentally verified in [10].

The time-of-flight t can be transformed to the distance-of-flight z using the relationship $z = L\tau/t$, where the time τ that has passed since the interaction is chosen. Values of τ and L are kept fixed. Substituting t by z, then the ion current density $j(L, t) = Q(L, t)\cdot v$ can be transformed to the space-resolved ion charge density at τ as [11]:

$$Q(z, \tau) = j(z)\tau L^3/z^4\,. \tag{4}$$

Since the ion expansion is closely related to the electron distribution, the ion density should decrease exponentially with distance. This can be expressed in a form $n_i(z,t) = n_0 \exp(-v/c_s)$, where $n_i(z,t)$ is the density for those ions traveling at velocity v, n_0 is the density at the emitting surface and c_s is the ion sound velocity [12]. Substituting $v = z/\tau$ gives:

$$n_i(z, \tau) = n_0 \exp\left(-\frac{z}{\tau c_s}\right), \tag{5}$$

where τ is the above-mentioned chosen time and $c_s=(kT_{ef}/M)^{1/2}$ is the ion sound velocity. kT_{ef} is generally a function of the charge state Z of ions, their temperature T_i and the temperature of electrons T_e. If T_{ef} does not change during the ion expansion, the experimentally obtained $n(z,\tau)$ follows single exponential decrease over the whole range. Considering $n_i(z,t) = Q_i(z,t)/e\bar{Z}$, where $\bar{Z}$ is the mean charge state of ions and e is the elementary charge, then the exponentially decreasing function $a_0 exp(-z/\tau c_s)$, where $a_0 = \bar{Z}en_0$, can be fitted to the experimentally obtained DOF spectrum to obtain corresponding value of c_s.

In conclusion, the ion sound velocity, which can be calculated from the exponential decay of the DOF spectra of ion charge density obtained by the transformation of the ion detector signals, can serve as a parameter suitable for scaling the properties of ions produced by lasers.

3. EXPERIMENTAL ARANGEMENT

The presented experiments were performed using two laser systems. The first laser was a COMpex 205 KrF excimer laser (Coherent) operating at 248 nm and irradiating targets with an intensity ranging from 10^8 to 10^{10} W/cm^2. Energy of a single 23-ns laser pulse can be varied up to 750 mJ. The laser pulse struck the target at 70° with respect to the target surface normal. The current of ions traveling through the vacuum chamber and drift tube was detected with the use of a Faraday cup (FC, an ion collector having the active area of 28.3 cm^2), which was positioned at 27.9 cm from the target surface along the target surface normal. For the applied FC bias voltage of −200 V the ion current was saturated. Targets as C, Cu, and Ta slabs of 0.1 to 0.2 mm in thickness were irradiated by laser pulses. The schematic of the experiment can be found elsewhere [13].

The second experiment was performed using the soft x-ray FEL FLASH2 and a Kirkpatrick-Baez focusing system with a focal length of 200 cm to focus 100-fs pulses of 20 - 100 μJ energy at 13.5-nm wavelength ($E_{ph} \approx 91.8$ eV) to a 36μm-sized spot surrounded by shallow lobes resulting in intensities reaching 10^{13} W/cm^2 in the focus position [14]. The slab targets of Al, Cu, Fe, Ni, Si, GaAs and PMMA, ranging in thickness from 0.1 to 1 mm, were mounted on a target holder actuated by a 3-axis translational manipulator. The angle of incidence of the laser beam on the target was 22.5°. Information about the pulse energy was obtained from an in-line gas monitor detector (GMD), prior to arrival of the pulses at the interaction region [15]. The crater characteristics were obtained with the use of Nomarski-type (DIC – differential interference contrast) microscopy.

Since the ion production during soft x-ray ablation was very weak, the emitted ions were detected with the use of an open electron multiplier (EM) type 119EM placed along the normal of the target surface at 24 cm from the target. This windowless electron multiplier equipped with Be-Cu dynodes was produced by the Thorn EMI Electron Tubes, UK. It has a Venetian blind structure, with a 10-slat entrance dynode with radiation aperture of 2.16 cm in diameter and a total of 17 dynodes. An operating voltage of –3 kV was applied to the first dynode while the input grid was grounded. Since the ion-induced emission of electrons from the first dynode depends not only on the surface quality of the dynode, but also on the captured ions, their potential and kinetic energy, EM calibration is needed [16]. Since we were unable to calibrate the gain of the open electron multiplier during this experiment, we used previous data [17] for the range of low ion kinetic energies encountered in our experiment to determine the value of this gain as 5×10^5.

4. EXPERIMENTAL RESULTS

The direct comparison of UV and x-laser ablation characteristics is based on the TOF transformation using the relationship $t_2 = (L_2/L_1)\, t_1$, where L_1=27.8 cm is the distance of the FC from the target. The voltage signals of both ion detectors are transformed into current densities using equation (3). The Cu target was irradiated with fluencies of 10 and 34 J/cm^2 delivered by the soft x-ray FEL and KrF laser, respectively. Although the difference between the fluences used is not large, the difference in Cu ion emission is pronounced. While the maximum ion current density produced by the KrF laser reaches ~4 mA/cm^2, it is only ~0.2 nA/cm^2 for Cu ions produced by the XFEL, as Figure 1a shows. The yields of ions represented by the total charge carried by the ions are in a similar ratio of $1{:}1\times10^{-7}$. It can be assumed that not only the ~300 times higher energy delivered to the target contributes to this, but above all the 23ns interaction of the KrF laser pulse with the ablated mass, which results in effective ionization with 5eV laser photons. In addition, laser energy deposited near the critical plasma density is thermally transported to denser and cooler regions at the target, causing greater material ablation and creating an inward ablation pressure. The ion yield and energy can also be increased by finding the optimal position of the laser focus, which is always in front of the target surface [18, 19]. On the contrary, the XFEL pulse produces ions with an order of magnitude greater velocity, both maximum and peak velocities, which corresponds to the maximum current amplitude. Figure 1b shows the corresponding TOF spectra calculated using equation (4) for a selected time of 100 ns. The ion charge density distribution along the target surface normal shows that the charge density of the fastest group of ions produced by the XFEL laser is 10^8 times lower than that produced by the KrF laser. This value is related to the measurable beginning of ion currents.

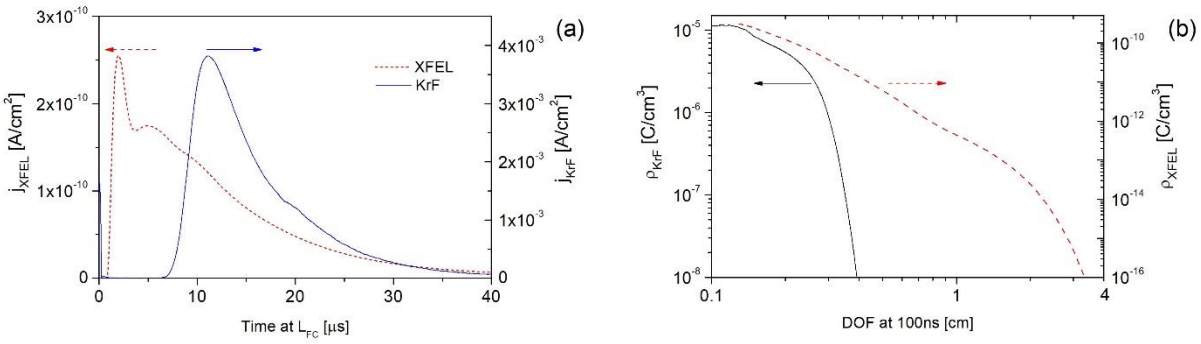

Figure 1. (a) Comparison of ion current densities emitted by a Cu target irradiated by 100fs-XFEL and 23ns-KrF laser delivering energy of 100 μJ and 34 mJ, respectively. The TOF spectra are related to the distance of the Faraday cup from the target, L_{FC} =27.9 cm. (b) Comparison of DOF spectra of charge density of Cu ions produced by XFEL and KrF laser calculated for 100 ns elapsed since interaction.

The higher energy component of the ion beams driven by both lasers is situated closer to the beam axis parallel to the front surface normal of the target. The quality of ion sources is assessed in terms of maximum energy and energy dispersion. The term maximum energy is related to the fastest ions located at the front of the expanding plasma. These fastest ions are not ionized atoms of the target material, but ionized hydrogen that comes from a layer of chemisorbed hydrocarbons and H_2O on the target surface. Ionized hydrogen, carbon and oxygen are easily identified in plasma production of heavy elements, especially tantalum. The inset in Figure 2a shows the time-resolved Ta current driven by the KrF laser, where 2

separate peaks of low amplitude occur before the dominant Ta ion peak current. The fastest peak is formed by H^+ ions, the second is composed of C^{Z+} and O^{Z+} ions. The transformation of the TOF spectrum to the DOF one using the relationship (4) allows highlighting these low amplitude peaks shown in Figure 2 for Ta and GaAs plasma produced with 23-ns KrF laser and 100-fs XFEL pulses, respectively. The three ranges of the DOF spectrum plotted semi-logarithmically in Figure 2a show an almost linearly decreasing charge density of Ta ions. This makes it possible to fit an exponentially decreasing function to the linear parts of the DOF spectrum and to determine the sound velocity of the ions according to equation (4). The fitted functions $a_0 exp(-z/\tau c_s)$ are represented by three lines in Figure 2a: The fits of dashed green, dash-dotted red and short dashed blue lines allowed to determine the value of $E_{fe} = \bar{Z}\, kT_e + kT_i$ of groups of ions with mean charge $\bar{Z}e$ [20] emerging in the given regions, for H^+, C^{Z+} and Ta^{Z+} ions. The fitting gave E_{fe} values of 4, 8 and 10 eV for H^+, C^{Z+} and Ta^{Z+} ions, respectively. The kinetic energy of Ta^{Z+} ions reaches the highest value due to their highest atomic mass M (4).

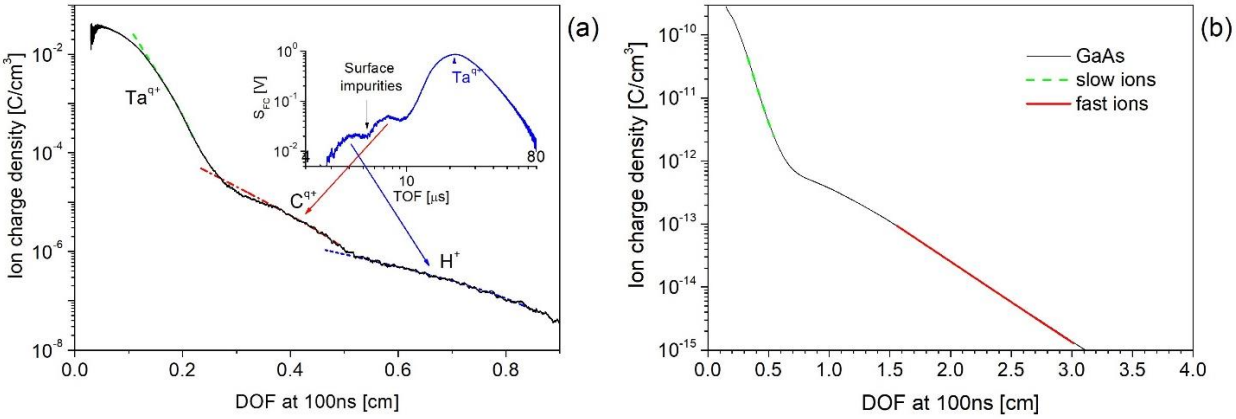

Figure 2. Spatial distribution of charge density of Ta and GaAs ions after 100 ns of irradiation by (a) 23ns KrF laser and (b) 100 fs XFEL, respectively. The inset in (a) shows the corresponding time-resolved ion current that has been transformed into DOF using relation (4).

Figure 3 shows the E_{fe} values for H^+ ions emitted from various materials exposed to XFEL and KrF laser radiation. H^+ ions produced by the XFEL laser have E_{fe} ~ 10 eV. In contrast, the E_{fe} value is about 200 times lower for H^+ ions produced by 23-ns KrF laser pulses for both the graphite and Cu targets. This large difference is due to the different effect of long and ultrashort lasers. While the nanosecond laser pulse interacts with the plasma expanding from the target and its energy is consumed by several processes, the energy of the femtosecond pulse is concentrated within the irradiated volume, which does not change during heating. Due to the high-pressure gradients, the irradiated material begins to expand freely picoseconds after the laser-target interaction.

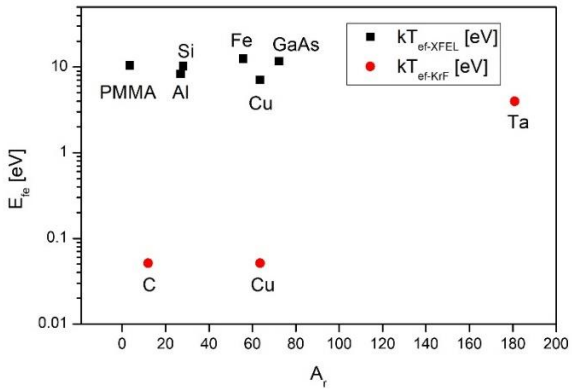

Figure 3. Values of E_{fe} determined from the ion sound velocity of H^+ ions emitted by plasma from different elements sorted by relative atomic mass A_r. Plasmas were produced by 100fs XFEL and 23ns KrF lasers heating the target surfaces with a fluence of 34 and 10 J/cm^2, respectively.

Figure 3 shows that E_{fe} of H^+ ions are independent on the target material up to relative atomic mass A_r ~80 for both experiments. H^+ ions originating from impurities chemisorbed on the surface of the tantalum target have E_{fe} ~ 4eV, which is about 10 times higher than in the case of graphite and Cu targets. This is related to their detachment from the Ta surface and the formation of a separated group of fast ions, as Figure 2a shows. Although the efficiency of energy transfer between electrons and heavy Ta^{Z+} ions could be assumed to be lower due to the large mass ratio, as might be expected when comparing the expansion velocity of ions into vacuum [20, 21], the kinetic energy of lighter impurity ions including H^+ is always smaller than the maximum ion energy of heavier elements of a bulk target. The phenomenon of complete separation is not pronounced in the case of ions with a smaller A_r value, as shown in Figure 3. In addition, the ionized impurities such as carbon ions are part of the fastest ion group of the target material.

One of the general characteristics of laser ablation is the dependence of the energy of the fastest ions (i.e., the "maximum ion energy") on the laser fluence. The data presented in Figure 4 showing the general trend of maximum ion energy versus fluence delivered by fs-ns lasers were collected from a series of experiments devoted to the ablation of thick planar targets, specifically according to the Wang diagram [22]. The solid line illustrates the trend of maximum kinetic energy vs. laser fluence for ions of different elements produced by different lasers in the wavelength range 193 - 1064 nm and pulse duration range 3 - 30 ns according to Wang. References to presented experiments are given to the right outside the diagram.

Despite the large dispersion, presented data show an increasing dependence of the maximum energy on laser fluence. At the centre of the data set, there is a large scattering of the maximum ion energy values. The vertically oriented line at a fluence of 10 J/cm^2 shows the maximum ion energy range from ~1 – 1000 eV. The horizontally oriented line shows that the maximum energy of 30 eV was achieved for fluence rage from 0.5 – 35 J/cm^2. This large dispersion of experimental data complicates the understanding of laser ablation. Vertical scattering at 10 J/cm^2 shows that unlike ns-lasers, the maximum energy of H^+ ions is effectively generated by 100fs XFEL pulses. However, the slowest H^+ ions were emitted from the ^{14}Si target, the fastest from the ^{28}Ni and ^{29}Cu targets. The maximum kinetic energy of Ni and Cu target ions produced in this experiment is about 50-60 times higher than that of H^+ ions (not shown in Figure 4). Compilation of data from other experiments with 15fs-XFEL (labels BI and JA) and 52fs-790nm laser pulses (label YO) also confirm more efficient coupling of laser energy into short-lived plasma via maximum energy of H^+ ions for fluences above 100 J/cm^2. However, it should be noted that production of MeV protons was achieved by enhanced coupling of laser energy to the plasma by creating a pre-plasma with the use of an ns-laser before the arrival of the main fs-pulse and by modifying target composition in the case of clusters or microdroplets and by the introduction of sub-laser-wavelength surface modulations on solid targets [26].

The maximum energy of H^+ ions emitted from the surface of graphite, Cu and Ta targets irradiated with the 23-ns KrF laser pulses increases with increasing atomic weight of the target elements. Also in this case, the mass ratio of produced ions affects the energy transfer between electrons and ions. H^+ ions from the Ta target were accelerated to a higher kinetic energy than H^+ from the graphite target. However, in contrast to the final energy E_{fe} of ions, this effect is already significant even for elements with $A_r < 80$. The estimated value of the maximum kinetic energy of Ta^{Z+} ions is about 20 times higher than that of the corresponding H^+ ions, and thus its value is higher than indicated by the solid trend line XW.

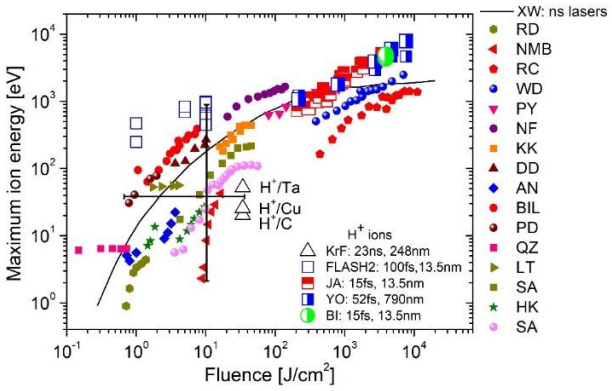

FIGURE 4 Compilation of data showing the dependence of ion energy to laser fluence in the high irradiance regime for fs-ns lasers. Line XW illustrates the general trend for ns-ablation of different elements by Wang [22]. Maximum energy of H^+ ions by femtosecond ablation of different target materials: BI [23], JA [24], YO [25]. Maximum energy of ions produced by nanosecond ablation of different target materials: RD [27], NMB [28], RC [29], WD [20], PY [30], NF [31], KK [32], DD [33], AN [34], BIL [35], PD [36], QZ [37], LT [38], SA [39], HK [40].

5. CONCLUSIONS

The fundamental difference between femtosecond and nanosecond laser-induced ablation processes is that the femtosecond laser pulse duration is shorter than the electron-ion energy transfer time and the heat conduction time in the sample lattice, while the nanosecond laser pulse interacts with the ablated material that remains in contact with the target. A comparison of the properties of ions produced by ablation induced by 100fs, 100μJ x-ray FLASH2 and 23ns, 34mJ KrF lasers provides the following conclusions:

1) Nanosecond UV ablation of bulk targets produces ~10^7 times more ions than femtosecond x-ray ablation.
2) The final energy of ions associated with the ion acoustic velocity driven by the soft x-ray laser is ~200 times higher than that of the UV ns-laser pulses.
3) The maximum energy of protons produced by the soft-x-ray laser is ~16 times higher than that of a UV ns-laser pulses.

In summary, the time-of-flight and distance-of-flight methods applied here for the analysis of ions emitted during fs- and ns-ablation of bulk targets represent a simple but effective tool contributing to the characterization and comparison of different mechanisms of laser energy dissipation in irradiated samples.

ACKNOWLEDGMENTS

This work is partly supported by the EURATOM within the "Keep-in-Touch" activities and the Aquitaine Regional Council. We acknowledge the financial support from the French National Research Agency (ANR) in the frame of "the Investments for the future" Programme IdEx Bordeaux-LAPHIA (ANR-10-IDEX-03-02), and the Czech Science Foundation (grants no. GM23-05027M and 20-08452S). Team of K. Falk funded by the Helmholtz Association under the grant no. VH-NG-1338. A.F., T.G., T.C., S.R., Y.S. and S.M.V. acknowledge support from the UK EPSRC grants EP/P015794/1 and EP/W010097/1, and from the Royal Society. J.K., L.J., M.K., T.B., Š.J. and S.K.S. acknowledge support from the Czech Ministry of Education, Youth and Sports (grant no. LM2023068).

REFERENCES

[1] V. A. Azov, L. Mueller, A. A. Makarov, Laser ionization mass spectrometry at 55: Quo Vadis?. Mass Spec. Rev. 41, 100–151 (2022). https://doi.org/10.1002/mas.21669.

[2] R. E. Russo, Laser ablation research and development: 60 years strong. Appl. Phys. A 129, 168 (2023). https://doi.org/10.1007/s00339-023-06425-3

[3] S. Preuss, A. Demchuk, M. Stuke, Sub-picosecond UV laser ablation of metals, Appl. Phys. A 61, 33-37 (1995). https://doi.org/10.1007/BF01538207.

[4] S. Amoruso, C. Altucci, R. Bruzzese, C. De Lisio, N. Spinelli, R. Velotta, M. Vitiello, X. Wang, Study of the plasma plume generated during near IR femtosecond laser irradiation of silicon targets. Appl. Phys. A 79, 1377–1380 (2004). https://doi.org/10.1007/s00339-004-2785-9

[5] R. Hergenröder, O. Samek, and V. Hommes, Femtosecond laser ablation elemental mass spectrometry. Mass Spec Rev 25, 551–572 (2006). https://doi.org/10.1002/mas.20077

[6] R.W. Lee, H.A. Baldis, R.C. Cauble, O.L. Landen, J.S. Wark, A. Ng, S.J. Rose, C. Lewis, D. Riley, J.-C. Gauthier, and P. Audebert, Plasma-based studies with intense X-ray and particle beam sources. Laser Part. Beams Beams 20, 527-536 (2002). DOI: https://doi.org/10.1017/S0263034602202293

[7] S. Preuss, A. Demchuk, and M. Stuke, Sub-picosecond UV laser ablation of metals. Appl. Phys. A 61, 33-37 (1995). https://doi.org/10.1007/BF01538207

[8] J. Chalupský et al., Spot size characterization of focused non-Gaussian x-ray laser beams, Opt. Express 18, 27836 (2010). https://doi.org/10.1364/OE.18.027836

[9] J. Chalupsky et al., Comparing different approaches to characterization of focused x-ray laser beams. Nucl. Instrum. Meth. A 631, 130 - 133 (2011). https://doi.org/10.1016/j.nima.2010.12.040

[10] J. Krása, L. Láska, K. Rohlena, M. Pfeifer, J. Skála, B. Králiková, P. Straka, E. Woryna and J. Wolowski, The effect of laser-produced plasma expansion on the ion population. Appl. Phys. Lett., 75, 2539-2541 (1999). https://doi.org/10.1063/1.125070

[11] J. Krása, P. Parys, L. Velerdi, A. Velyhan, L. Ryć, D. Delle Side, and V. Nassisi, Time-of-flight spectra for mapping of charge density of ions produced by laser. Laser Part. Beams (2014), 32, 15–20. doi:10.1017/S0263034613000797

[12] T. H. Tan, G. H. McCall, and A. H. Williams, Determination of laser intensity and hot-electron temperature from fastest ion velocity measurement on laser-produced plasma, Phys. Fluids 27, 296 - 301 (1984). https://doi.org/10.1063/1.864482

[13] L. Velardi, D. Delle Side, J. Krása and V. Nassisi, Proton extraction from transition metals using PLATONE. Nucl. Instrum. Meth. A 735, 564 - 567 (2014). https://doi.org/10.1016/j.nima.2013.10.013

[14] M. Manfredda et al., The Evolution of KAOS, a multipurpose Active Optics System for EUV/Soft x-rays. In: Synchrotron Radiation News 0.0 (2022), pp. 1–8. https://doi.org/10.1080/08940886.2022.2066432

[15] A. A. Sorokin et al., An x-ray gas monitor for free-electron lasers. J. Synchrotron Rad. 26, 1092 - 1100 (2019). https://doi.org/10.1107/S1600577519005174

[16] HP. Winter, H. Eder, and F. Aumayr, Kinetic electron emission in the near-threshold region studied for different projectile charges. International Journal of Mass Spectrometry 192 (1999) 407–413. https://doi.org/10.1016/S1387-3806(99)00074-3

[17] J. Krasa, M. Pfeifer, M. P. Stöckli, U. Lehnert, and D. Fry, The effect of the first dynode's geometry on the detection efficiency of a 119EM electron multiplier used as a highly charged ion detector. Nucl. Instr. and Meth. B 152, 397 - 402 (1999). https://doi.org/10.1016/S0168-583X(99)00173-1

[18] L. Láska, K. Mašek, B. Králiková, J. Krása, J. Skála, K. Rohlena, E. Woryna, J. Wol/owski, K. Langbein, and H. Haseroth, Highly charged Ta ions produced by the photodissociation iodine laser with subnanosecond pulses. Appl. Phys. Lett. 65, 691 - 693 (1994). http://dx.doi.org/10.1063/1.113017

[19] Y. Wada, Y. Shigemoto and A. Ogata. Ion production enhancement by rear-focusing and prepulse in ultrashort-pulse laser interaction with foil targets. AIP Conf. Proc. 737, 832–838 (2004). https://doi.org/10.1063/1.1842630

[20] W. Demtröder, W. Jantz, Investigation of laser-produced plasmas from metal surfaces. Plasma Phys. 12, 691 -0703 (1970). DOI 101088/0032-1028/12/9/004.

[21] H. Y. Zhao, J. J. Zhang, Q. Y. Jin, W. Liu, G. C. Wang, L. T. Sun, X. Z. Zhang, and H. W. Zhao, New development of laser ion source for highly charged ion beam production at Institute of Modern Physics. Rev. Sci. Instrum. 87, 02A917 (2016). http://dx.doi.org/10.1063/1.4937115

[22] X.Wang, S. Zhang, X. Cheng, E. Zhu, W. Hang, B. Huang, Ion kinetic energy distributions in laser-induced plasma. Spectrochimica Acta Part B: Atomic Spectroscopy, 99 (2014) 101-114, http://dx.doi.org/10.1016/j.sab.2014.06.018.

[23] B. Iwan et al., TOF-OFF: A method for determining focal positions in tightly focused free-electron laser experiments by measurement of ejected ions. High Energy Density Phys. 7, 336e342 (2011). doi:10.1016/j.hedp.2011.06.008

[24] J. Andreasson et al., Saturated ablation in metal hydrides and acceleration of protons and deuterons to keV energies with a soft-x-ray laser. Phys. Rev. E 83, 016403 (2011). https://doi.org/10.1103/PhysRevE.83.016403.

[25] Y. Okano, H. Kishimura, Y.Hironaka, K. G. Nakamura, and K. Kondo, X-ray and fast ion generation from metaltargets bz femtosecond laser irradiation. Appl. Surf. Sci. 197-198, 281-284 (2002). https://doi.org/10.1016/S0169-4332(02)00383-5

[26] S. Bagchi, P. Prem Kiran, M.K. Bhuyan, S. Bose, P. Ayyub, M. Krishnamurthy, and G.R. Kumar, Fast ion beams from intense, femtosecond laser irradiated nanostructured surfaces. Appl. Phys. B 88, 167–173 (2007). https://doi.org/10.1007/s00340-007-2706-7.

[27] R. Dreyfus, Cu^0, Cu^+, and Cu2 from excimer-ablated copper, J. Appl. Phys. 69, 1721–1729 (1991). https://doi.org/10.1063/1.347218

[28] N. M. Bulgakova, A.V. Bulgakov, O.F. Bobrenok, Double layer effects in laser-ablation plasma plumes, Phys. Rev. E. 62, 5624 - 5635 (2000). https://doi.org/10.1103/PhysRevE.62.5624

[29] R. W. Coons, D. Campos, M. Crank, S. S. Harilal, A. Hassanein, Comparison of EUV spectral and ion emission features from laser-produced Sn and Li plasmas, Proc. SPIE 7636, 763636 (2010). https://doi.org/10.1117/12.848318

[30] P. Yeates, C. Fallon, E. Kennedy, J.T. Costello, Charge resolved electrostatic diagnostic of colliding copper laser plasma plumes. Phys. Plasmas 18, 103104 (2011). https://doi.org/10.1063/1.3633486

[31] N. Farid, S. Harilal, H. Ding, A. Hassanein, Kinetics of ion and prompt electron emission from laser-produced plasma. Phys. Plasmas 20, 073114 (2013). https://doi.org/10.1063/1.4816710

[32] K. Koivusaari, J. Levoska, S. Leppävuori, Pulsed-laser deposition of diamond-like carbon: relations between laser fluence, velocity of carbon ions, and bonding in the films. J. Appl. Phys. 85, 2915–2920 (1999). https://doi.org/10.1063/1.369057

[33] D. Doria, A. Lorusso, F. Belloni, V. Nassisi, L. Torrisi, S. Gammino, A study of the parameters of particles ejected from a laser plasma. Laser Part. Beams 22, 461–467 (2004). https://doi.org/10.1017/S0263034604040108

[34] A. Narazaki, T. Sato, Y. Kawaguchi, H. Niino, Plume dynamics of iron disilicide studied by time-of-flight mass spectroscopy. Appl. Surf. Sci. 208, 52–56 (2003). https://doi.org/10.1016/S0169-4332(02)01335-1

[35] B. Ilyas, A. Dogar, S. Ullah, A. Qayyum, Laser fluence effects on ion emission from a laser-generated Cu plasma. J. Phys. D. Appl. Phys. 44, 295202 (2011). http://dx.doi.org/10.1088/0022-3727/44/29/295202

[36] P. Dyer, R. Greenough, A. Issa, P. Key, Spectroscopic and ion probe measurements of KrF laser ablated Y–Ba–Cu–O bulk samples. Appl. Phys. Lett. 53, 534–536 (1988). https://doi.org/10.1063/1.100628

[37] Q.-Z. Qin, Z.-H. Han, H.-J. Dang, An angle-resolved time-of-flight mass spectrometric study of pulsed laser ablated Ta_2O_5. J. Appl. Phys. 83, 6082–6088 (1998). https://doi.org/10.1063/1.367478

[38] L. Torrisi, F. Caridi, D. Margarone, A. Picciotto, A. Mangione, J. Beltrano, Carbon plasma produced in vacuum by 532 nm–3 ns laser pulses ablation. Appl. Surf. Sci. 252, 6383–6389 (2006). https://doi.org/10.1016/j.apsusc.2006.01.042

[39] S. Amoruso, M. Armenante, V. Berardi, R. Bruzzese, N. Spinelli, Absorption and saturation mechanisms in aluminium laser ablated plasmas. Appl. Phys. A 65, 265–271 (1997). https://doi.org/10.1007/s003390050577

[40] H. Köster, K. Mann, Influence of beam parameters on the laser induced particle emission from surfaces. Appl. Surf. Sci. 109, 428–432 (1997). https://doi.org/10.1016/S0169-4332(96)00780-5